The influence of solution treatment on the phase evolution and tensile properties of binary Ti-Mo alloys

by N.A. Moshokoa[1,2], M.L. Raganya[1,2], R. Machaka[1,2], M.E. Makhatha[2], and B.A. Obadele[3]

Affiliation:
[1]Advance Materials and Engineering, Manufacturing Cluster, Council for Scientific and Industrial Research, Brummeria, Pretoria,South Africa
[2]Department of Metallurgy, School of Mining, Metallurgy and Chemical Engineering, University of Johannesburg, Doornfontein Campus, Johannesburg, South Africa
[3]Department of Chemical, Materials and Metallurgical Engineering, Botswana International University of Science and Technology, Botswana

Correspondence to:
B.A. Obadele

Email:
obadele4@gmail.com

Dates:
Received: 1 Sept. 2020
Revised: 8 Mar. 2021
Accepted: Feb. 2024
Published: May 2024

How to cite:
Moshokoa, N.A., Raganya, M.L., Machaka, R., Makhatha, M.E., and Obadele, B.A. 2024. The influence 0f solution treatment on the phase evolution and tensile properties of binary Ti-Mo alloys. *Journal of the Southern African Institute of Mining and Metallurgy*, vol. 124, no. 5. pp. 253–262

DOI ID:
http://dx.doi.org/10.17159/2411-9717/1354/2024

ORCID:
B.A. Obadele
http://orcid.org/0000-0003-4529-4762
N.A. Moshokoa
http://orcid.org/0000-0001-5750-1314
M.L. Raganya
http://orcid.org/000-0002-3259-8647
R. Machaka
http://orcid.org/0000-0002-3174-8703
M.E. Makhatha
http://orcid.org/0000-0003-2157-9712

Abstract

The influence of solution treatment on the phase evolution and tensile properties of Ti-Mo alloys was investigated to assess their potential use in biomedical applications. Phase formation and microstructural evolution were studied using X-ray diffraction (XRD), optical microscopy (OM), scanning electron microscopy (SEM), and electron backscatter diffraction (EBSD). The mechanical properties were characterized by means of tensile tests and bending strength. XRD analysis showed that solution treatment increased the volume fraction of β phase and supressed the α" phase. The microstructures of the as-cast alloys consisted of β equiaxed grains with sub-grain structures of different sizes, while the solution treated alloys comprised β equiaxed grains only except for Ti-10.02Mo, which comprised needle-like α" structures. EBSD showed an increase in the volume fraction of the ω and α" phases in all the alloys after solution treatment. The elastic modulus and UTS of all the alloy significantly decreased after solution treatment, except for Ti-15.05Mo, whereas the elongation significantly increased. The fracture surfaces of all the alloys after solution treatment indicated more ductile behaviour than brittle.

Keywords

Ti-Mo alloys, solution treatment, mechanical properties, microstructure

Introduction

Biomedical implants made of natural or artificial materials have been developed over the years to replace lost or diseased biological structures and improve quality of life (Long and Rack, 1998; Geetha et al., 2009; Gepreel and Niinomi, 2012). Navarro, Michiardi, and Castan (2008) reported that the use of implants has become more widespread, especially in aged people suffering from conditions such as arthritis and joint pains. According to Long and Rack (1998), orthopaedic hip and knee joint replacements have a high prevelance due to factors such as osteoarthritis (inflammation in the bone joints), osteoporosis (weakening of the bones), and trauma, which can lead to pain, loss of function, or loss of natural healing ability. However, the effectiveness of implants can be compromised by factors such as debris generation, metal ion release and foreign body response, and mismatch of modulus between the bones and the implant or low strength under load (Gepreel and Niinomi, 2013).

The design and development of orthopaedic materials must take into account certain requirements to avoid revision surgery. An elastic modulus close to that of the bone to avoid the stress shielding effect is vital. The stress shielding effect (Engh and Bobyn, 1988) is insufficient load transfer from the artificial implant to the adjacent remodelling bone, which leads to bone resorption and eventually loosening of the prosthetic. Due to this considerations, metals and alloys have been extensively used as load-bearing implants. For example, Ti6Al4V is commonly used for prostheses such as knee joint and hip replacements because of its outstanding properties such as high specific strength, excellent corrosion resistance, low elastic modulus, and superior biocompatibility compared to stainless steel and Co-Cr materials (Sidambe, 2014). However, the advantages of this alloy are not sufficient to avoid implant failure, because Ti6Al4V suffers from two major drawbacks. The release of Al and V ions is reported to cause adverse health issues. (Okazaki, 1996; Keda et al., 2002). Also, Ti6Al4V has a modulus of 110 GPa, higher than that of human bone at 10-40 GPa (Niinomi, 2008).

Therefore, the development and design of β-type Ti alloys containing non-toxic and non-allergenic elements such as Mo, Nb, Ta, Zr, and Sn has attracted considerable attention because of their properties such as low elastic modulus and excellent biocompatibility. In this study, commercially pure Ti was micro-alloyed with molybdenum (Mo) due to its strong β-stabilizing properties and low cost compared with other β-stabilizing elements (Polmear, 2006; Lu et al., 2013). Currently, the binary alloys Ti-10Mo, Ti-15Mo, and

The influence of solution treatment on the phase evolution and tensile properties of binary

Ti-7.5Mo have been developed for use in biomedical applications in the as-cast condition. Most previous studies on Ti-Mo alloys have concentrated on phase transformations, microstructure, and mechanical properties in the as-cast condition and there are few studies on these properies in solution-treated alloys. Therefore, the aim of this study was to investigate the influence of solution treatment of the microstructure and tensile properties of Ti-10.02Mo, Ti-10.83Mo, Ti-12.89Mo, and Ti-15.05Mo.

Experimental

Alloy design and preparation

The cluster-plus-glue-atom-model was used to design the compositions of the Ti-Mo binary alloys. The β-stabilizing prediction tools found in the literature, such as molybdenum equivalence (Mo_{eq}), valence electron to atom (e/a) ratio, and the d-electron stability map were used to forecast the stability of the β phase. Mo_{eq} is defined as the total number of beta-stabilizing elements, alpha-stabilizing elements, and neutral elements required to retain 100% of the β phase after quenching from above the β transus temperature to room temperature (Welsch, Boyse, and Collings, 1993). Bania (1994) reported that a Mo_{eq} value of 10.0 wt% in Ti-Mo alloys is required to stabilize the β phase during quenching. The e/a ratio is the average number of valence electron in each atom of Ti-Mo binary alloys and is used to predict the formation of athermal omega (ω) phase in Ti alloys. According to Ikehata et al. (2004) the formation of athermal omega phase is at its maximum at an e/a ratio of 4.13 and minimum at 4.30; above this minimum the β phase becomes dominant. The calculated values of Mo_{eq} and e/a showed that all the designed alloys will stabilize the β phase upon quenching without precipitation of the ω phase.

The phase stability map was used to predict the stability of the β phase in Ti-Mo alloys upon quenching from the beta transus. According to the phase stability map, Ti-10.02Mo is located between the martensitic and the ω phase boundary lines, indicating that it will form β+α"+ω upon quenching above the beta transus. Ti-10.83Mo is between the slip line and the ω boundary line, meaning that after quenching the alloy will include β+ω. The Ti-12.89Mo alloy is situated in the β field, suggesting that the alloy will contain β phase only. The Ti-15.05Mo alloy is positioned in the β field, implying that it will comprise only β phase upon quenching from above the beta transus region. The calculated Mo equivalences, e/a ratios, bond order (Bo) and mean d-orbital energy level (Md) values are presented in Table I, while their positions are indicated on the Bo and Md stability map in Figure 1.

Processing

Elemental powders of CP-Ti and molybdenum were fabricated to produce ingots of 100 g each. A cold-press machine was employed to produce green compacts, which were melted in a water-cooled copper crucible with a tungsten electrode using a commercial arc melting vacuum-pressure casting system. Prior to melting, the melting chambers were evacuated and purged with argon. The ingots were re-melted three times to ensure chemical homogeneity. The as-cast ingots were solution treated at a temperature of 1100°C for an hour and then quenched in icy water.

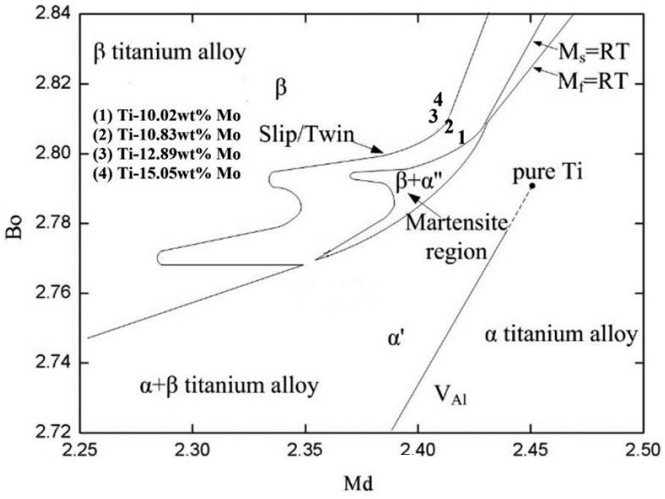

Figure 1—The Bo and Md stability phase map showing the positions of the designed alloys (Kuroda et al., 1998)

Phase and microstructural analysis

The samples were prepared for microstructural analysis following standard metallographic techniques used for Ti and its alloys. The samples were etched with Kroll's reagent (92 ml distilled water, 8 ml HNO_3, and 2 ml HF) for 60 secongs. The microstructure was examined using an optical microscope (Leica CTR4000) and scanning electron microscope (Joel: JSM-6510). Phase analysis was done using a Philips PANalytical powder diffractometer configured with an X'Celerator detector. The patterns were run with Co-Kα radiation with a secondary monochromatic wavelength of λ = 1.89 Å. Phase identification was done using X'Pert HighScore software as well as available literature for comparison. Samples for EBSD analysis were electropolished using a Struers polishing machine. Electron backscatter diffraction (EBSD) scans were performed using a Zeiss Crossbeam 540 instrument operating at 25 kV and 10 nA to image the samples. The EBSD analyses were performed using an Oxford NordLys Max³ detector and Oxford Aztec analysis software.

Mechanical properties

Tensile test specimens with gauge dimensions of 3 × 4 × 10 mm were sectioned from the ingots using electrical discharge machining (EDM). Tensile tests were performed using the Instron™ 1342 apparatus at room temperature. The strain was measured using an extensometer. Three samples from each alloy were tested for mechanical properties (UTS, *E*, %e) and the average of the three was calculated.

Table I

Nominal compositions and calculated values of Mo_{eq}, e/a ratio, and Bo and Md

Cluster formula	Composition [wt.%]	Mo_{eq} (wt.%)	e/a ratio	Bo	Md
$[(Mo)-(Ti)_{14}]\ Ti_4$	Ti-10.02 Mo	10.02	4.20	2.804	2.4215
$[(Mo)-(Ti)_{14}]\ Ti_{2.5}$	Ti-10.83 Mo	10.83	4.24	2.806	2.4188
$[(Mo)-(Ti)_{14}]\ Mo_{0.1}\ Ti0.9$	Ti-12.89 Mo	12.89	4.26	2.809	2.4133
$[(Mo)-(Ti)_{14}]\ Mo_{0.3}\ Ti0.7$	Ti-15.05 Mo	15.05	4.30	2.812	2.4077

Results

XRD analysis

X-ray diffraction was conducted to identify the constituent phases of the Ti-Mo alloys in the as-cast (Moshokoa, 2021) and solution treated conditions. The XRD patterns are presented in Figure 2. The diffreactogram of Ti-10.02Mo (Figure 2a) indicates high volume fractions of orthorhombic martensite (α" peaks) and low volume fractions of the bcc phase (β peaks) in the as-cast condition and after solution treatment. The highest peak (i.e., α") was found to be 2θ = 49°. The Ti-10.83Mo alloy (Figure 2b) shows higher intensity peaks of the α" phase and few peaks of bcc β phase in the as-cast condition. After solution treatment, there was transformation of α" into β phase at 2θ = 68° and 85°. The higher volume fraction peaks of α" phase may be due to the martensitic start (Ms) temperature, which is above room temperature during casting and quenching and the Mo composition being too low to supress the Ms temperature. The Ti-12.89Mo alloy (Figure 2c) shows a lower volume fraction of the orthorhombic martensitic α" phase than Ti-10.02Mo and Ti-10.83Mo in the as-cast condition. The β phase peaks are more prominent after solution treatment, with a single peak of α" present at 2θ = 75°. The highest peak is that of bcc β phase at 2θ = 46°. The paucity of α" peaks in the as-cast condition and the single peak after solution treatment may be attributed to the decrease in the Ms temperature to close to room temperature. Figure 2d illustrates equal volume fractions of orthorhombic martensitic α" phase and bcc β phase in the as-cast condition. After solution treatment, the XRD pattern shows bcc β phase peaks only, with the highest peak

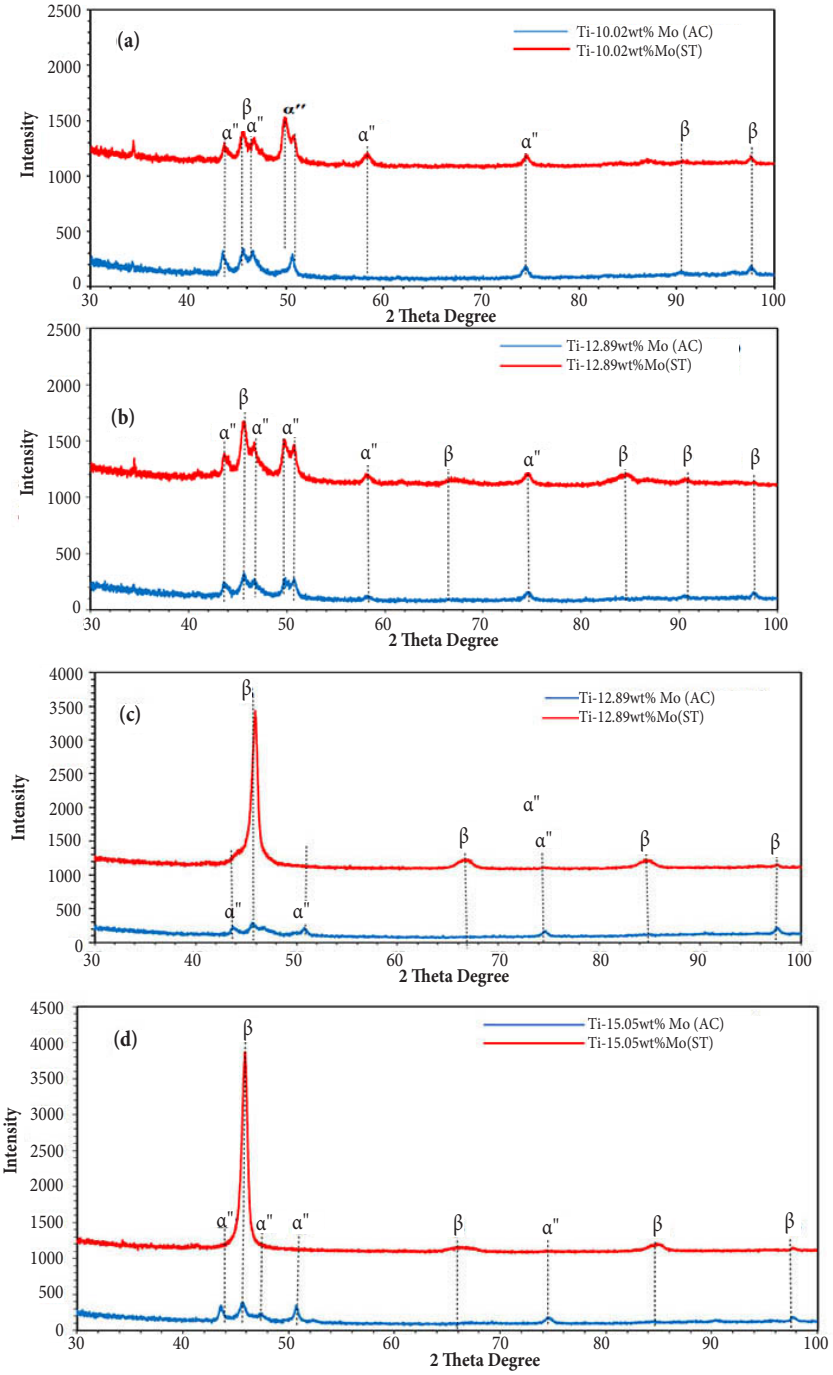

Figure 2—XRD patterns of (a) Ti-10.02Mo, (b) Ti-10.83Mo, (c) Ti-12.89Mo, and (d) Ti-15.05Mo alloys in as-cast (AC) and solutiontreated (ST) conditions

at around 2θ = 46°. The significant decrease in the orthorhombic martensitic peaks in the as-cast condition is attributed to the significant decrease in the Ms temperature, and the presence of the β phase peaks only after solution treatment is due to the Ms temperature being at room temperature during quenching and the molybdenum content being high enough to supress the α" phase. The ω phase was below the detection limit in all of the samples.

The XRD results for Ti-10.02Mo in the as-cast condition are consistent with the results reported by Oliveira and Guastaldi (2008) but different from those reported by Bania (1994), who stated that the β phase is retained at a Mo content of 10 wt%. The XRD results for Ti-15.05Mo alloy are also inconsistent with the results reported by Martins et al. (2011).

None of the as-cast Ti-Mo alloys are in agreement with the experimental results reported by Chen et al. (2006), Ho, Ju, and Lin (1999), and Davis, Flower, and West (1979). The XRD spectrum for as-cast Ti-12.89Mo is quite different from results reported by Oliveira and Guastaldi (2009) and Ho, Ju, and Lin (1999) where an α" peak is found at 2θ = 76°. The XRD results of the solution-treated Ti-10.02Mo and Ti-15.05Mo alloys are in agreement with the results reported by Cardoso et al. (2014) and Wang et al. (2016).

Zhao et al. (2012) also reported the presence of β phase in Ti-15Mo. The phase constituents of all the designed alloys in the as-cast condition differ from the theoretical results in Table I and Figure 1. The results of the solution-treated Ti-10.02Mo, Ti-10.83Mo, and Ti-12.89Mo also differ from the theoretical results. However, solution-treated Ti-15.05Mo agrees with all the theoretical results. The Mo equivalence and the e/a ratio predict that the β phase will be retained after quenching above the β transus temperature without the precipitation of the secondary phases. The average Bo and Md stability map predicts that Ti-10.02Mo and Ti-10.83Mo will exhibit β, α", and ω phases upon quenching from above the β transus temperature, whereas Ti-12.89Mo and Ti-15.05Mo are predicted to form only the β phase.

Optical micrography

Figure 3 depicts the optical micrographs of the alloys in the as-cast and solution-treated conditions. Ti-10.02Mo consists of equiaxed β grains and sub-grain boundaries in both the as-cast and solutiontreated conditions (Figure 3a and 3b). The Ti-10.83Mo alloy contains β equiaxed grains with fewer sub-grain boundaries than Ti-10.02Mo in the as-cast condition. After solution treatment, the alloy consists of β equiaxed grains only. As-cast Ti-12.89Mo has a similar structure to Ti-10.83Mo, although with a lower volume fraction of sub-grain boundaries. The solution-treated microstructure is similar to Ti-10.83Mo. The Ti-15.05Mo alloy in the as-cast condition is comparable to Ti-10.83Mo and Ti-12.89Mo alloys, with a significant decrease in the sub-grain boundaries. The solution-treated micrographs show only β equiaxed grains.

The significance reduction in the sub-grain boundaries with increasing Mo content in the as-cast alloys may be due to a decreasing s Ms temperature. The presence of a martensitic phase is also reported in other studies as evidence for martensitic transformation from β to α" phase (Mantani, 2006; Ho, 2008). The exceptional suppression of α" in Ti-10.83Mo, Ti-12.89Mo, and Ti-15.05Mo after solution treatment shows that the Ms temperature is below room temperature during quenching.

The microstructures obtained for all the alloys are quite different from those reported by Chen et al. (2006) and Ho, Ju, and Lin (1999). However, as-cast Ti-10.02Mo alloy is in agreement with the findings of Chen et al. (2006), Moshokoa et al. (2019), and Raganya et al. (2021). The presence of a martensitic phase is also reported in other studies as evidence for a martensitic transformation from a β to an α"phase (Mantani, 2006). The Ti-10.02Mo (ST) alloys are in agreement with Wang et al. (2016) but differ from the findings of Cardoso et al. (2014). However, the Ti-15.05Mo (ST) alloy is consistent with experimental results reported by Zhao et al. (2012), Cardoso et al. (2014), and Wang et al. (2016). Due to the paucity of work reported on solution-treated Ti-10.83Mo and Ti-12.89Mo, it is challenging to compare the experimental results with those reported in the literature.

The optical micrographs of all the designed alloys in as-cast conditions are in contrast with the theoretical results predicted by the Mo equivalence, e/a ratio, and the d-electron methods. The Ti-10.02Mo and Ti-10.83Mo alloys after solution treatment are not consistent with the theoretical results, especially the average Bo and Md stability map, whereas micrographs of the solution-treated Ti-12.89Mo and Ti-15.05Mo alloys are in agreement with the theoretical results predicted by the β stabilizing method.

EBSD maps

The EBSD technique was utilized to further characterize the phase constituents and microstructures of the alloys. The EBSD inverse

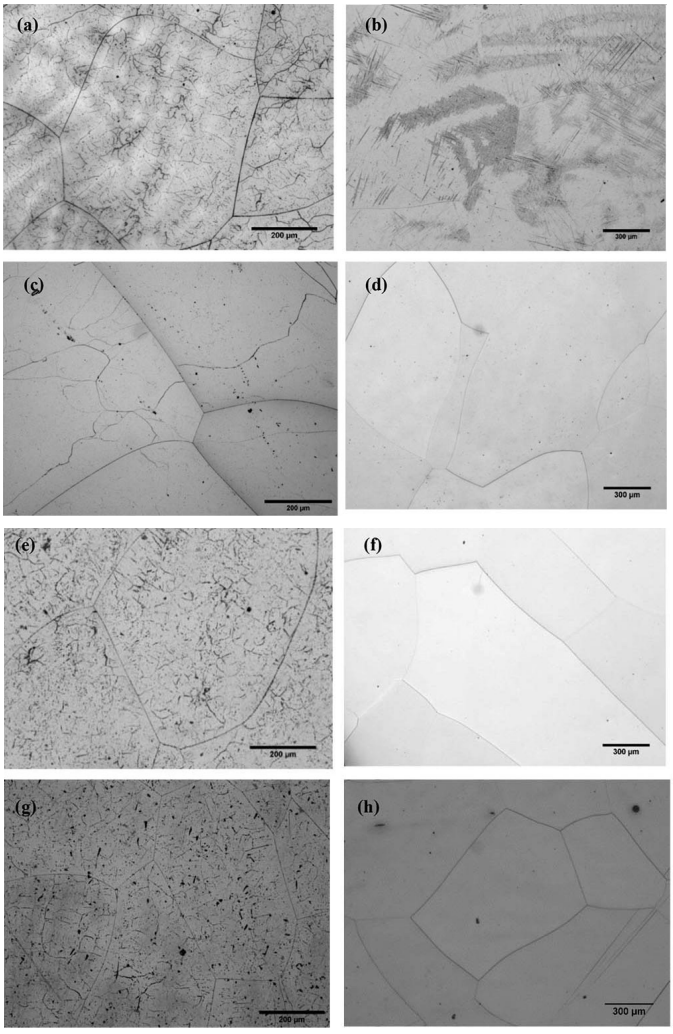

Figure 3—Optical micrographs of Ti-10.02Mo (a) as-cast and (b) solution-treated, Ti-10.83Mo (c) as-cast and (d) solution-treated, Ti-12.89Mo (e) as-cast and (f) solution-treated, and Ti-15.05Mo (g) as-cast and (h) solution-treated

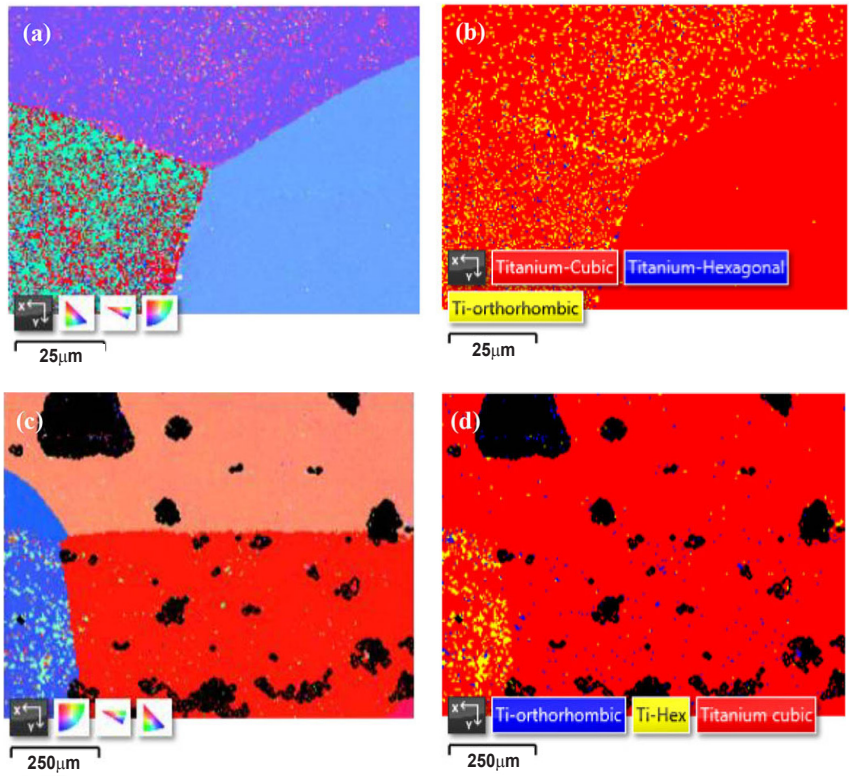

Figure 4—EBSD IPF and phase maps of Ti-10.02Mo alloy in (a, b) as-cast and (c, d) solution-treated conditions

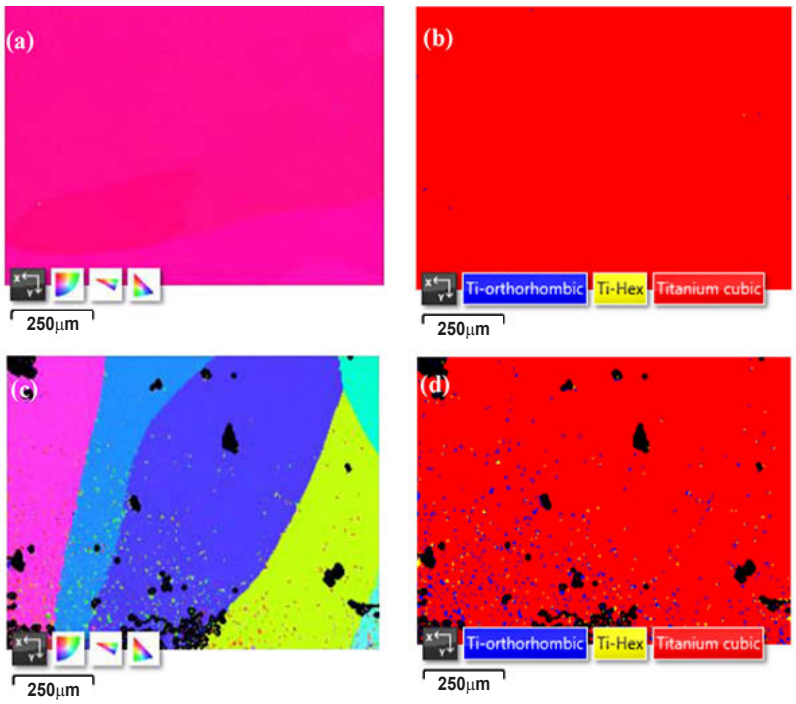

Figure 5—EBSD IPF and phase maps of Ti-10.83Mo in (a, b) as-cast and (c, d) solution-treated conditions

pole figures (IPFs) and phase maps of the as-cast and solution-treated alloys are presented in Figures 4–7. The IPF maps at different orientations show the grain boundaries and small grains of different colours within the large grains. The particles in as-cast Ti-10.02Mo and Ti-15.05Mo are identified as bcc β phase as the matrix in a red colour, orthorhombic martensitic α" represented in a yellow colour, and the ω phase illustrated in a blue colour, while the Ti-10.83Mo and Ti-12.89Mo alloys were identified as bcc β phase as the matrix (red), orthorhombic martensitic α" (blue), and the ω phase (yellow). The particles after solution treatment for all the alloys were distinguished as β phase as the matrix (red), orthorhombic martensitic α" (blue), and the ω phase (yellow) colour.

The Ti-10.02Mo alloy in the as-cast condition (Figure 4b) exhibited a high volume fraction of the ω phase and orthorhombic

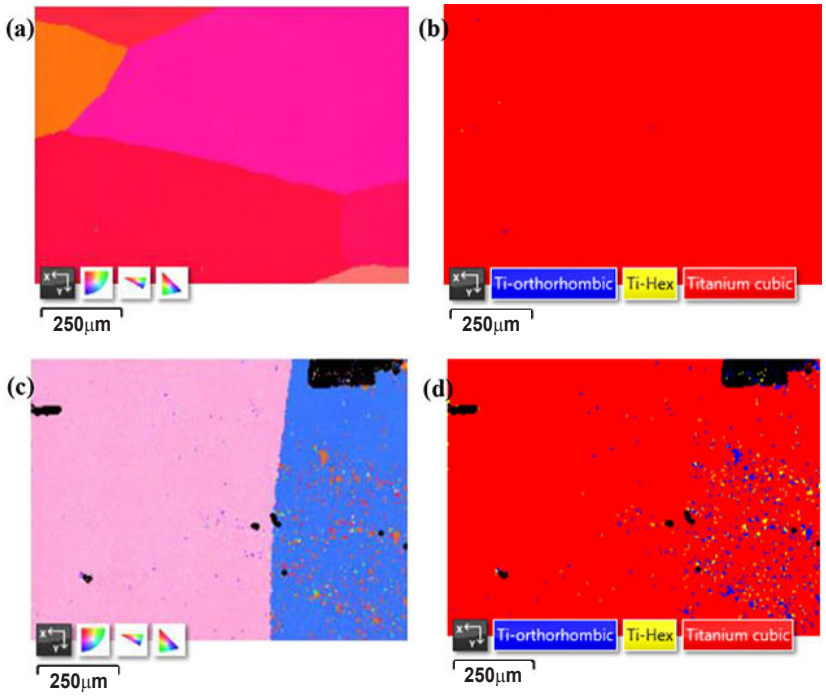

Figure 6—EBSD IPF and phase maps of Ti-12.89Mo alloy in (a, b) as-cast and (c, d) solution-treated conditions

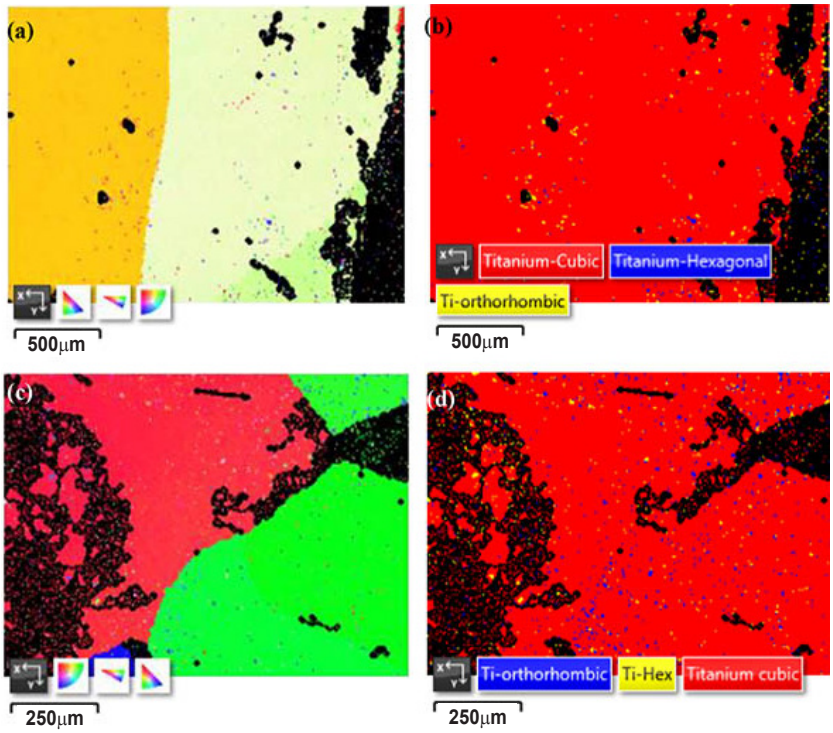

Figure 7—EBSD IPF and phase maps of Ti-15.05Mo alloy in (a, b) as-cast and (c, d) solution-treated conditions

martensitic precipitate. After solution treatment the fraction of orthorhombic martensitic precipitates decreased while the ω precipitates increased, as shown in Figure 4d. Ti-10.83Mo and Ti-12.89Mo in the as-cast condition (Figures 5b and 6b) show minor ω and α" precipitates distributed unevenly through the grains. The amount of the precipitates was too low to distinguish them clearly, and this may be caused by segregation during cooling. After solution treatment, the alloy shows a high volume fraction of α" precipitates and a low volume fraction of ω precipitates (Figures 5d and 6d respectively). The volume fractions of both the ω and martensitic phase in Ti-10.02Mo and Ti-12.89Mo alloys increased significantly in the as-cast condition and after solution treatment. The as-cast Ti-15.05Mo alloy (Figure 7b) shows lower contents of α" and ω precipitates compared to Ti-10.02Mo alloy. After solution treatment the volume fractions of the ω and α" precipitates increased significantly compared to the other alloys (Figure 7d. The orthorhombic martensitic phase and the ω phase were heterogeneously distributed along the β equiaxed grains in all the alloys. It was difficult to distinguish the secondary phases in some of the grains, and this may be attributed to segregation.

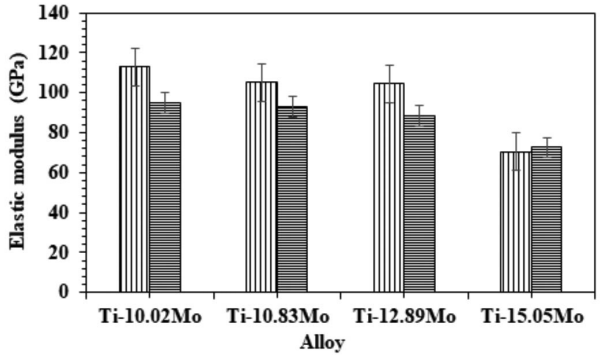

Figure 8—Elastic moduli of Ti-Mo alloys in as-cast (AC) and solution-treated (ST) conditions

The occurrence of the ω phase in EBSD maps is not widely reported in the literature, especially in as-cast and solution-treated binary Ti-Mo alloys, therefore it was challenging to compare these experimental results with those of previous work. Further research is required to quantify the use of this technique in characterizing the ω phase.

Tensile properties

Elastic modulus

The elastic moduli of the alloys are illustrated in Figure 8. The Ti-10.02Mo alloy in the as-cast condition exhibited the highest elastic modulus, and after solution treatment the elastic modulus decreased significantly. The high elastic modulus in the as-cast alloy may be attributed to the presence of ω precipitates as observed in the EBSD map (Figure 4b). The elastic moduli of as-cast Ti-10.83Mo and Ti-12.89Mo were found to be higher than the values after solution treatment. This may be due to the higher volume fraction of the ω phase, although ω was not detected, due to segregation during cooling. The decrease in the elastic modulus as the Mo content increased is due to the stability of the β phase and the suppression of the orthorhombic martensitic α"phase, which is evident in the XRD spectra and optical micrographs. The elastic modulus of Ti-15.05Mo increases after solution treatment. This may be attributed to the substantial increase in the volume fraction of ω precipitates, as seen in the EBSD phase map in Figure 7d. Lee and Ju (2002) reported that the phases influence the elastic modulus in the order $E_\omega > E_{\alpha'} > E_{\alpha''} > E_\beta$. It is noted that the ω phase has a higher elastic modulus than the β and martensitic α"phases. Likewise, it is well known that the ω phase has a significant effect on the mechanical properties of Ti alloys, and it is likely to increase the elastic modulus (Akahori, Niinomi, and Fukui, 2005). Graft, Levinson, and Rostoker (1957) also indicated that the ω phase had an unusually high elastic modulus. Hao et al. (2006) also reported that the ω phase is deleterious to the mechanical properties as it increases the elastic modulus.

The elastic moduli of the as-cast Ti-Mo alloys are lower than for commercially available Ti6Al4V as reported by Niinomi (2008). It was difficult to compare the findings of the present study with the values for Ti-Mo alloys reported by Ho, Ju, and Lin (1999) in as-cast conditions and Ti-Sn alloys because they reported on the bending modulus only, whereas the elastic modulus results in this work were obtained from tensile tests. The elastic moduli of the alloys after solution treatment were lower than commercially available Ti6Al4V alloy as reported by Niinomi (1986). The elastic moduli of the Ti-10.02Mo and Ti-15.05Mo alloys are lower than those reported by Zhou and Luo (2011a), Cardoso et al. (2014), and Wang et al. (2016) in the solution-treated condition.

Ultimate tensile strength and elongation

The ultimate tensile strength and elongation data are presented in Table II. As-cast Ti-10.02Mo exhibited a higher UTS after solution treatment. This may be due to the decrease in the ω phase, s shown in Figure 4. The elongation increased significantly after solution treatment, indicating that the as-cast alloy was too brittle. The results reported by Wang et al. (2016) for Ti-10.02Mo alloy after solution treatment show an enhanced UTS (756.17 MPa) and percentage elongation (24.04%) compared to the studied alloy. The UTS of Ti-10.83Mo decreased after solution treatment but the elongation increased significantly. The UTS of solution-treated Ti-12.89Mo was lower than in the as-cast alloy. The elongation of the Ti-12.89Mo alloy in the as-cast condition was significantly lower, indicating that the alloy was too brittle, whereas the Ti-12.89Mo alloy after solution treatment displayed a significantly higher elongation, which indicates that the alloy was more ductile. The UTS and elongation of Ti-15.05Mo alloy in the as-cast condition werelower, and increased significantly after solution treatment. The increase in the UTS may be attributed to the increase in the ω precipitates, as seen in the EBSD phase map in Figure 7d. The elongation indicates improved ductility after solution treatment. The UTS and elongation of the Ti-10.02Mo and Ti-15.05Mo alloys after solution treatment were found to be lower than the values reported by Wang et al. (2016), but higher than reported by Zhou and Luo (2011b). The elongation reported by Zhou and Luo was higher

Table II

Tensile properties of as-cast (AC) and solution treated (ST) alloys

Alloy	UTS (AC) MPa	UTS (ST) MPa	%E (AC)	%E (ST)
Ti-10.02Mo	764.42	684.65	0.92	20.17
Ti-10.83Mo	885.45	764.22	0.35	26.15
Ti-12.89Mo	726.34	718.23	0.22	16.60
Ti-15.05Mo	593.48	705.91	0.35	6.95
Ti-10Mo (Wang et al., 2016)	-	756.17	-	24.04
Ti-15Mo (Wang et al., 2016)		739.38		29.02
Ti-15Mo (Zhou et al., 2012)		680		49

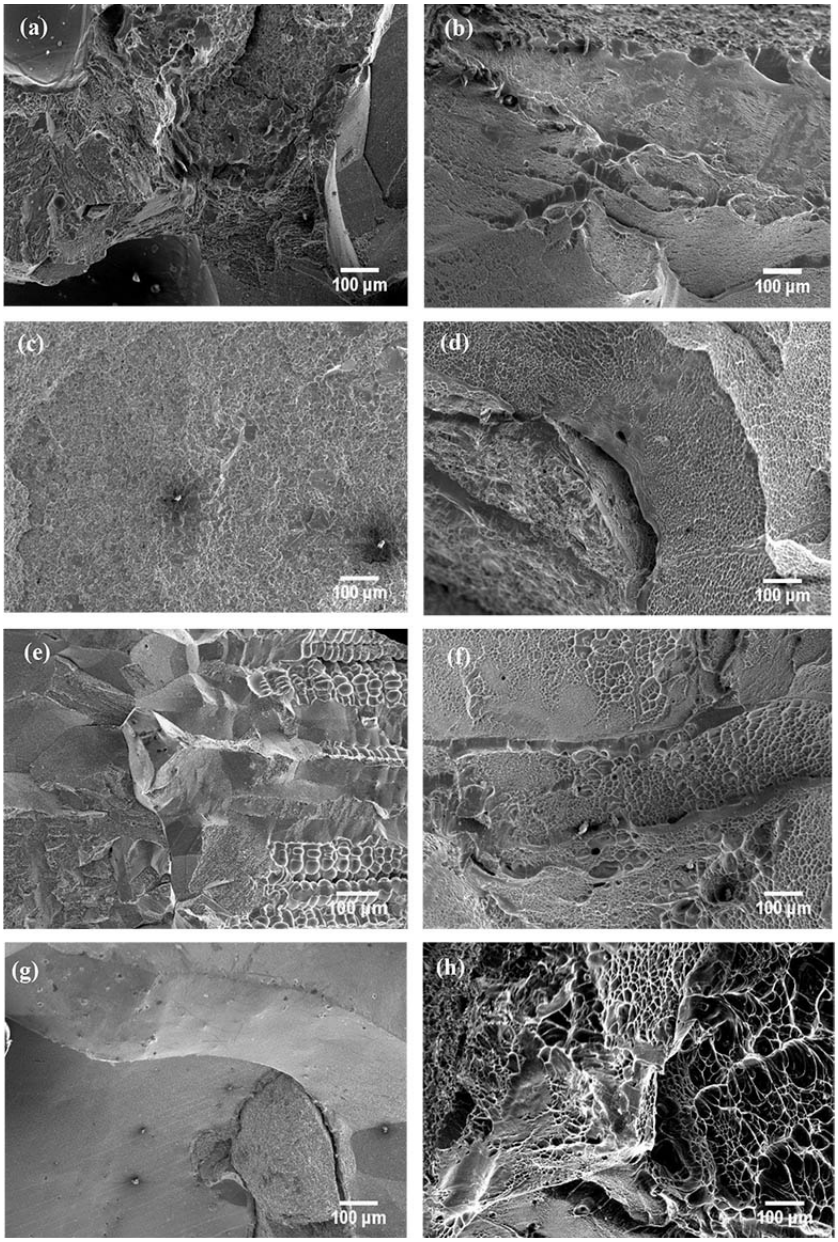

Figure 9 —Fracture surfaces of Ti-10.02Mo (a) as-cast and (b) solution-treated, Ti-10.83Mo (c) as-cast (c) and (d) solution-treated, Ti-12.89Mo (e) as-cast and (f) solution treated, and Ti-15.05Mo (g) as-cast and (d) solution treated

than that of the designed alloy, though. In general, Ti-10.83Mo showed moderate strength and high elongation, which is desirable for biomedical applications. However, the elastic modulus was still higher than that of human bone.

Figure 9 displays SEM micrographs of the fracture surfaces of the alloys after tensile testing. Ti-10.02Mo alloy in the as-cast condition exhibits both dimples and cleavage facets, indicating that the alloy undergoes both brittle and ductile fracture. However, the pronounced cleavage facets show that brittle fracture is the dominant mode of failure. Solution-treated Ti-10.02Mo alloy shows numerous smooth cleavage facets on the fractured surface, which is an indication of a typical brittle fracture. Ti-10.83Mo alloy in the as-cast condition shows small dimples without cleavage facets, implying ductile fracture. After solution treatment, the fracture surface exhibits small dimples with subordinate cleavage facets, indicating high ductility and ductile fracture. Likewise, as-cast Ti-12.89Mo shows more cleavage features with lesser dimpling. After solution treatment, the fracture surface consists of medium dimples with cleavage facets, indicating both ductile and brittle fracture, together with dendrites that may have formed due to casting porosity. Ti-15.05Mo alloy shows dominant cleavage features with a small amount of dimple features. After solution treatment, the fracture surface is characterized by large dimples and fewer cleavage facets, indicating a dustile fracture even though the ductility of the alloy has decreased. The fracture surfaces of the Ti-10.02Mo and Ti-15.05Mo alloys differ from those obtained by Wang et al., (2016), who reported that the alloys were characterized by ductile fracture only.

Conclusion

The characteristics of the as-cast alloys obtained by XRD, optical microscopy, and EBSD were found to be inconsistent with the results predicted using β stabilizing predictions. The optical

microscopy results for solution-treated Ti-10.83Mo, Ti-12.89Mo, and Ti-15.05Mo were in agreement with the theoretical results, but the Ti-10.02Mo results were inconsistent. The XRD results for the solution-treated alloys were not in agreement with the theoretical results, except for Ti-15.05Mo. The XRD patterns of all the alloys in the as-cast condition indicated the presence of both orthorhombic martensitic and bcc β phase, with increasing transformation of α" to β after solution treatment. Ti-15.05Mo alloy was able to retain the β phase. The ω phase was not detected by XRD in any of the alloys, either as-cast or solution-treated, due to the detection limit.

The optical micrographs of all the designed alloys in the as-cast condition showed β equiaxed grains sub-grains of different sizes. The solution-treated Ti-10.83, Ti-12.89Mo, and Ti-15.05Mo alloys comprised only β equiaxed grains, whereas the Ti-10.02Mo alloy showed needle like structures in addition to the β equiaxed grains. The EBSD phase maps of all the designed alloys showed an increase in the ω and orthorhombic precipitates after solution treatment. The elastic moduli and UTS of all the designed alloys decreased significantly, except for Ti-15.05Mo, for which both the elastic modulus and UTS increased slightly after solution treatment. The ductility of all the designed alloys improved significantly after solution treatment, and this was also evident in the SEM micrographs of the fracture surfaces. These alloys show promise in advancing dental implant materials. However, further testing on their biocompatibility, mechanical properties, and bio/tribocorrosion resistance is required to verify their suitability for implant applications.

Acknowledgements

We acknowledge NRF Thuthuka (Grant No: 115859) for funding this project, the CSIR for laboratory facilities, the casting team at Mintek, and the University of Pretoria laboratory and CSIR teams for assisting with the work. We also thank our supervisors, Dr Babatunde Abiodun Obadele, Ms Lerato Raganya, Professor Ronald Machaka, and Professor Elizabeth Makhatha for their supervision.

Author contribution

NAM: Conceptualization, characterization of the samples, manuscript writing, editing of the manuscript.
R: Conceptualization, characterization, and editing.
RM: Conceptualization and editing.
MEM: Conceptualization and editing.
BAO: Supervision, conceptualization, editing and final checks or editing.

References

Akahori, Y., Niinomi, M., Fukui, H., Ogawa, M., and Toda, H. 2005. Improvement in fatigue characteristics of newly developed beta type titanium alloy for biomedical applications by thermo-mechanical treatments'. *Material Science and Engineering C*, vol. 25, no. 3, pp. 248–254. doi: 10.1016/j.msec.2004.12.007

Bania, P.J. 1994. Beta titanium alloys and their role in the titanium industry. *JOM*, vol. 46, pp. 16–19.

Cardoso, F.F., Ferrandini, P.L., Lopes, E.S.N., Cremasco, A., and Caram, R. 2014. Ti–Mo alloys employed as biomaterials: Effects of composition and aging heat treatment on microstructure and mechanical behavior. *Journal of the Mechanical Behavior of Biomedical Materials*, vol. 32, pp. 31–38. doi: 10.1016/j.jmbbm.2013.11.021

Chen, Y-Y., Xu, L-J., Liu, Z-G., Kong, F-T., and Chen, Z. 2006. Microstructures and properties of titanium alloys Ti-Mo for dental use. *Transactions of Nonferrous Metals Society of China*, vol 16, pp. 824–828. doi: https://doi.org/10.1016/S1003-6326(06)60308-7

Davis, R., Flower, H.M., and West, D.R.F. 1979. Martensitic transformations in Ti-Mo alloys. *Journal of Materials Science*, vol. 14, no. 3, pp. 712–722. doi: 10.1007/BF00772735

Engh, C.A. and Bobyn, J.D. 1988. The influence of stem size and extent of porous coating on femoral bone resorption after primary cementless hip arthroplasty. *Clinical Orthopaedics and Related Research*, vol. 231, pp. 7–28.

Geetha, M., Singh, A.K., Asokamani, R., and Gogia, A.K. 2009, Ti based biomaterials, the ultimate choice for orthopaedic implants–a review. *Progress in Materials Science*, vol. 54, no. 3, pp. 397–425.

Gepreel, M.A-H. and Niinomi. M. 2013. Biocompatibility of Ti-alloys for long-term implantation, *Journal of the Mechanical Behavior of Biomedical Materials*, vol. 20, pp. 407–415. doi: 10.1016/j.jmbbm.2012.11.014

Graft. W.H., Levinson, D.W., and Rostoker, W. 1957. The influence of alloying on the elastic modulus of titanium alloys. *Transactions of Nonferrous Metals Society of China*.

Hao, Y.L., Li, S.J., Sun, S.Y., and Yang, R. 2006. Effect of Zr and Sn on Young's modulus and superelasticity of Ti–Nb-based alloys. *Material Science and Engineering A*, vol. 441, no, 1–2, pp. 112–118. doi: 10.1016/j.msea.2006.09.051

Ho, W. 2008. Effect of omega phase on mechanical properties of Ti-Mo alloys for biomedical applications. *Journal of Medical and Biological Engineering*, vol. 28, no. 1, p. 47.

Ho, W.F., Ju, C.P., and Lin, J.HC. 1999 Structure and properties of cast binary Ti-Mo alloys. *Biomaterials*, vol. 20, no. 22, pp. 2115–2122.

Ikehata, H., Nagasako, N., Furuta, T., Fukumoto, A., Miwa, K., and Saito, T. 2004. First-principles calculations for development of low elastic modulus Ti alloys. *Physical Review B*, vol. 70, no. 17, p. 174113. https://journals.aps.org/prb/abstract/10.1103/PhysRevB.70.174113

Keda, Y.M. , Krjukova, I,V., Ilovalskala, I.A., Morozova, M.A., Gofanova, O.V., Babarina, M.V., Marova, E.I., Pankov, Y.A., and Kandror, V.I. 2002, Antibodies to pituitary surface antigens during various pituitary disease states. *Journal of Endocrinology*, vol. 175, no. 2, pp. 417–423.

Kuroda, D., Niinomi, M., Morinaga, M., Kato, Y., and Yashiro, T. 1998. Design and mechanical properties of new β type titanium alloys for implant materials. *Materials Science and Engineering A*, vol, 243, no. 1-2, pp. 244–249.

Lee, C.M., Ju, C.P., and Chern Lin, J.H. 2002. Structure-property relationship of cast Ti-Nb alloys. *Journal of Oral Rehabilitation*, vol. 29, no. 4, pp. 314–322. doi: 10.1046/j.1365-2842.2002.00825.x

Long, M. and Rack, H.J. 1998. Titanium alloys in total joint replacement — a materials science perspective. *Biomaterials*, vol. , no. 18, pp. 1621–1639.

Lu, J-W., Zhao, Y-Q., Ge, P., and Niu, H-Z. 2013. Microstructure and beta grain growth behavior of Ti–Mo alloys solution treated. *Materials Characterization*, vol. 84, no. 96, pp. 105–111. doi: 10.1016/j.matchar.2013.07.014

Mantani, Y. and Tajima, M. 2006. Phase transformation of quenched α" martensite by aging in Ti–Nb alloys. *Materials Science and Engineering A*, vol. 438–440, pp. 315–319. doi: 10.1016/j.msea.2006.02.180

Martins, J.R.S. Nogueira, R.A., de Araújo, R.O., Donato, T.A.G., Arana-Chavez, V.E., Claro, A.P.R.A., Moraes, J.C.S., Buzalaf, M.A.R., and Grandini, C.R. 2011. Preparation and characterization of Ti-15Mo alloy used as biomaterial. *Materials Research*, vol. 14, no. 1, pp. 107–112. doi: 10.1590/S1516-14392011005000013

Moshokoa, N., Raganya, L., Obadele, B., Olubambi, P., and Machaka, R. 2019. Effects of Mo content on the microstructural and mechanical properties of as-cast Ti-Mo alloys. *IOP Conference Series:* Materials Science and Engineering, vol. 655, no. 1, p. 012015.

Moshokoa, N.A., Raganya, M.L., Machaka, R., Makhatha, M.E., and Obadele, B.A. 2021. The effect of molybdenum content on the microstructural evolution and tensile properties of as-cast Ti-Mo alloys. *Materials Today Communications*, vol. 27, p.102347.

Navarro, M., Michiardi, A., Castaño, O., and Planell, J,A, 2008. Biomaterials in orthopaedics. *Journal of the Royal Society Interface*, vol. 5, no. 27, pp. 1137–1158. doi: 10.1098/rsif.2008.0151

Niinomi, M. 2008. Mechanical biocompatibilities of titanium alloys for biomedical applications. *Journal of the Mechanical Behavior of Biomedical Materials*, vol. 1, no. 1, pp. 30–42. doi: 10.1016/j.jmbbm.2007.07.001

Niinomi, M., Adachi,. M., and Kobayashi, T. 1986. Evaluation of toughness in 7075 alloy by R curve method. *Journal of Japan Institute of Light Metals*, vol. 36, no. 4, pp. 215–222. doi: 10.2464/jilm.36.215w

Okazaki, Y. 1996. Corrosion resistance and corrosion fatigue strength of new titanium alloys for medical implants without V and Al. *Materials Science and Engineering A*, vol. 213, no. 1–2, pp. 138–147.

Oliveira, N.T.C. and Guastaldi, A.C. 2008. Electrochemical behavior of Ti-Mo alloys applied as biomaterial. *Corrosion Science*, vol. 50, no. 4, pp. 938–945. doi: 10.1016/j.corsci.2007.09.009

Oliveira, N.T.C. and Guastaldi, A.C. 2009. Electrochemical stability and corrosion resistance of Ti–Mo alloys for biomedical applications. *Acta Biomaterialia,* vol. 5, no. 1, pp. 399–405. doi: 10.1016/j.actbio.2008.07.010

Polmear, I.J. 2006. Light Alloys: From Traditional Alloys to Nanocrystals. 4th edn. Butterworth-Heinemann. 421 pp.

Raganya, L., Moshokoa, N., Obadele, B.A., Olubambi, P.A., and Machaka, R. 2021. Investigation .of the tensile properties of heat treated Ti-Mo alloys. *Materials Today: Proceedings*, vol. 38, pp.1044–1048.

Sidambe, A.T. 2014. Biocompatibility of advanced manufactured titanium implants—A review. *Materials*, vol. 7, no. 12. doi: 10.3390/ma7128168

Wang, C.H., Yang, C.D., Liu, M., Li, X., Hu, P.F., Russell, A.M., and Cao, G.H. 2016. Martensitic microstructures and mechanical properties of as-quenched metastable β-type Ti–Mo alloys. *Journal of Materials Science*, vol. 51, pp. 6886–6896. doi: 10.1007/s10853-016-9976-6

Wang, X., Zhang, L., Guo, Z., JIang, Y., Tao, X., and Liu, L. 2016. Study of low-modulus biomedical β Ti-Nb-Zr alloys based on single-crystal elastic constants modeling. *Journal of the Mechanical Behavior of Biomedical Materials*, vol 62, pp. 310–318. doi: 10.1016/j.jmbbm.2016.04.040

Welsch, G., Boyse, R., and Collings, E.W. 1993. Materials Properties Handbook: Titanium Alloys. ASM International, Materials Park, OH.

Zhao, X., Niinomi, M., Nakai, M., and Hieda, J. 2012. Beta type Ti–Mo alloys with changeable Young's modulus for spinal fixation applications. *Acta Biomaterialia*, vol. 8, no. 5, pp. 1990–1997. doi: 10.1016/j.actbio.2012.02.004

Zhou, Y. and Luo, D. 2011a. Corrosion behavior of Ti–Mo alloys cold rolled and heat treated, *Journal of Alloys and Compounds*, vol. 509, no. 21, pp. 6267–6272. doi: 10.1016/j.jallcom.2011.03.045

Zhou, Y. and Luo, D. 2011b. Microstructures and mechanical properties of Ti–Mo alloys cold-rolled and heat treated. *Materials Characterization*, vol. 62, no. 10, pp. 931–937. doi: 10.1016/j.matchar.2011.07.010 ◆